Uplift Mechanism of Rectangular Tunnel in Liquefied Soils

Chung-Jung Lee, Yue-Chen Wei, Wen-Ya Chuang, Wen-Yi Hung, Wen-Lung Wu and Tai-Yuan Ho

Abstract Underground structures located in liquefiable soil deposits are susceptible to floating during earthquakes. These damage cases have been observed in huge earthquake events. A series of centrifuge tunnel model shaking table tests was conducted to investigate the uplift behaviour of rectangular tunnel embedded in liquefiable soils. The test results show that the buried depth of tunnel, the input amplitude of base acceleration and the number of loading cycles all influence the magnitude of tunnel uplift displacement. The higher hydraulic gradient between the soil beneath the tunnel bottom and the surrounding soil became obvious and the surrounding soil squeezing into the tunnel bottom is the major cause of tunnel uplifting. According to the analysis of model test results, the following conclusions are addressed: (1) Magnitude of tunnel uplift is significantly influenced by the viscosity of pore fluid used in the tests (less permeability of soil) and the embedded depth of tunnel. The tunnel would experience the less uplift if the tunnel is embedded in the deeper depth and in the less viscous pore fluid (higher permeability of soil). (2) Once the tunnel begins floating the liquefied sand will squeeze into the tunnel bottom due to high seepage forces from the outside of tunnel and the deeper soils below the tunnel towards the bottom of tunnel. (3) Once the safety factor against uplift (FS) calculated with the proposed method is less than 1 the tunnel would start floating and FS back to 1 the tunnel would stop floating during shaking.

Keywords Uplift mechanism of tunnel · Liquefaction · Centrifuge shaking table test

C.-J. Lee (✉) · Y.-C. Wei · W.-Y. Chuang · W.-Y. Hung
Department of Civil Engineering, National Central University,
Jhongli, Taoyuan, Taiwan
e-mail: cjleeciv@ncu.edu.tw

W.-L. Wu · T.-Y. Ho
CECI Engineering Consultants, Inc., Taipei, Taiwan

1 Introduction

Loose saturated sands are susceptible to generating larger excess pore water pressures during earthquakes, leading to a loss in the sand stiffness and strength. Investigations into damage sites after earthquakes reveal that soil liquefaction is one of the major factors that contribute to severe damage to buildings, oil tanks, bridges, tunnels, embankments, buried pipelines and marine structures (Abdoun et al. 2005; Lee 2005). Underground structures located in liquefiable soil deposits are susceptible to floating up during earthquakes and have been observed in recent major earthquake events (Tobita et al. 2010, 2012; Chian and Madabhushi 2010, 2012).

In Taipei city, an underground conduit was constructed between the Banchia railway station and the Taipei railway station to make way for both the Taiwan railway and the Taiwan high-speed railway systems, thereby, reducing the interference of these systems with road traffic. This tunnel was constructed using a cut-and-cover method. Two parallel slurry walls 36 m in depth and 1 m thick were built first, and the parallel walls with a bracing system were used to support the surrounding soils during soil excavation to a 17 m deep. Finally, the tunnel was constructed. The completed tunnel was enclosed by two parallel walls. Because parts of this tunnel route passed through liquefiable soils, the possibility of tunnel uplift and lateral displacement as a result of lateral spreading and/or liquefaction during larger earthquakes raised concerns after an upgrade of the design peak ground acceleration (PGA). As a result, it became necessary to re-evaluate the seismic behaviour of the liquefiable sand between the parallel walls, as well as the protective effects of the two parallel walls against uplift of tunnel and lateral spreading. In this paper, the uplift mechanism of rectangular tunnel during earthquake-induced liquefaction is major concern.

In situ investigations of liquefaction phenomena are difficult because earthquakes occur infrequently and unpredictably. Small-scale physical modelling provides an alternative to geotechnical earthquake engineering and has been used to gain insights into failure mechanisms. Geotechnical modelling requires the reproduction of the strength and stiffness associated with soil behaviour. Soil behaviour strongly depends on stress levels and stress histories. Centrifuge modelling enables complex scenarios to be reproduced at small scales and at low costs. The use of a soil with a soil density ρ both in a prototype and in a centrifuge model subjected to an inertial acceleration field of N times the earth's gravity yields a vertical stress at a depth h_m (the subscript m denotes the centrifuge model) that is identical to that of the corresponding prototype at a depth h_p (the subscript p denotes the prototype), where $h_p = Nh_m$. The model: prototype scale factor for linear dimensions is 1: N. This relationship is the scaling law of the centrifuge modelling; that is, the stress and pressure similarities are achieved at homologous points. The scaling relationships were applied to a prototype subjected to base shaking (the amplitude of the base acceleration, a_p, and the frequency, f_p) in the earth's gravity ($1g$), such that the corresponding $1/N$ centrifuge model was tested at an acceleration of Ng and subjected to base shaking (where the amplitude of acceleration is $a_m = Na_p$ and the

frequency is $f_m = Nf_p$). The scale factors that retained the stress and pressure similarities of the linear dimensions and base acceleration, a, of the centrifuge model and the prototype were $1:N$ and $1:N^{-1}$, respectively. A series of centrifuge tunnel model shaking table tests at an acceleration of $80g$ was conducted to investigate the uplift mechanism of rectangular tunnel embedded at different depths in liquefiable soils.

2 Centrifuge Modelling

2.1 Testing Equipment, Tested Sand, and Preparation of Sand Beds

This study was conducted in the Centrifuge at the National Central University (NCU), Taiwan. The NCU Centrifuge has a nominal radius of 3 m and has a 1-D servo-hydraulically controlled shaker integrated into a swing basket (Lee et al. 2012). The shaker has a maximum nominal shaking force of 53.4 kN with a maximum table displacement of ±6.4 mm and operates up to an acceleration of $80g$. The nominal operating frequency range of shaking is 0–250 Hz. The table-payload mounting area is 1000 mm × 546 mm × 500 mm. Fine quartz sand was used to prepare the sand beds. The characteristics of the fine quartz sand used are summarized in Table 1. A laminar container (711 mm (L) × 356 mm (W) × 353 mm (H)) was used to contain the sand deposits. The quartz sand was pluviated with a regular path into the container from a hopper at a fixed falling height and at a constant flow rate to prepare fairly uniform sand beds with a relative density of 55 %. The internal friction angle of tested sand bed was about 35.7°. The air pluviation process was interrupted as required for embedding the model tunnel, the accelerometers and pore water pressure transducers (PPTs) at specified elevations and locations. The prepared sand deposit was saturated with water or viscous fluid (kinematic viscosity ≈ 40 cSt) by a vacuum method.

2.2 Design and Fabrication of Model Tunnel

The prototype dimensions of the cross section of the rectangular rail tunnel are 9.15 m × 18 m ($h_p \times b_p$). The model tunnel was tested at an acceleration of $80g$,

Table 1 Characteristics of fine quartz sand

	G_s	D_{50} (mm)	D_{10} (mm)	[a]ρ_{max} (g/cm^3)	[a]ρ_{min} (g/cm^3)
Quartz sand	2.65	0.193	0.147	1.66	1.44

[a]The maximum and minimum densities of the sand were measured in the dry state, according to the method (JSF T 161-1990) specified by the Japanese Geotechnical Society
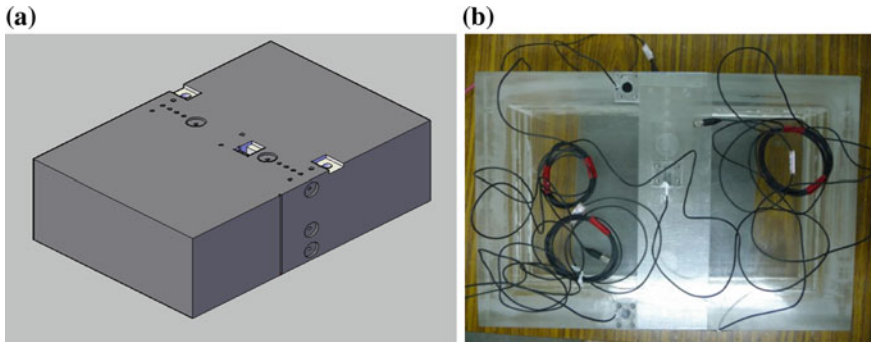
Fig. 1 Model tunnel: **a** 3-D model tunnel image; **b** model tunnel with instrumented transduces inside

therefore, the dimensions of model tunnel are scaled to 1/80 in length and are 0.114 m × 0.225 m ($h_m \times b_m$) per the centrifuge scaling law. Here h, b are the tunnel height and tunnel width, respectively. The suffixes $_m$ and $_p$ represent the dimension in model scale and in prototype scale. The unit weight of model tunnel including the transducers (accelerometers, pore water pressure transduces, and earth pressure cells) instrumented and embedded inside the model tunnel is 9.02 kN/m^3 and is nearly the same as the unit weight of in situ concrete tunnel including the railway and the other facilities (8.85 kN/m^3). The model tunnel was made of acrylic as shown in Fig. 1. The surface on the model tunnel was roughed with sand paper. The earth pressure cells, pore water pressure transducers, and accelerometer were instrumented on the 4-side surfaces to monitor the seismic responses of model tunnel subjected to the base shaking.

2.3   Testing Set-up and Testing Conditions

Figure 2a–c show the soil profiles and the instrumentation layouts used in the models. The dimensions in Fig. 2a–c are in centimeters, and the prototype dimensions in parentheses are in meters. Table 2 is the list of test number and testing conditions used in the study. Pore water pressure transducers (PPT#), earth pressure cells (EPC#), and accelerometers (A#) were instrumented in and around the model tunnel to monitor the changes of excess pore water pressure, the earth pressures and the accelerations on the surfaces and inside of model tunnel. Two vertical arrays of accelerometer and of pore water pressure transducer was also instrumented at the middle and right-hand side of the tunnel model in the sand deposit to capture the seismic response as clear as possible. All the accelerometers, EPCs, PPTs and LVDTs were mounted in an effort to measure the following seismic responses of model: (1) Tunnel uplift displacement; (2) Ground surface
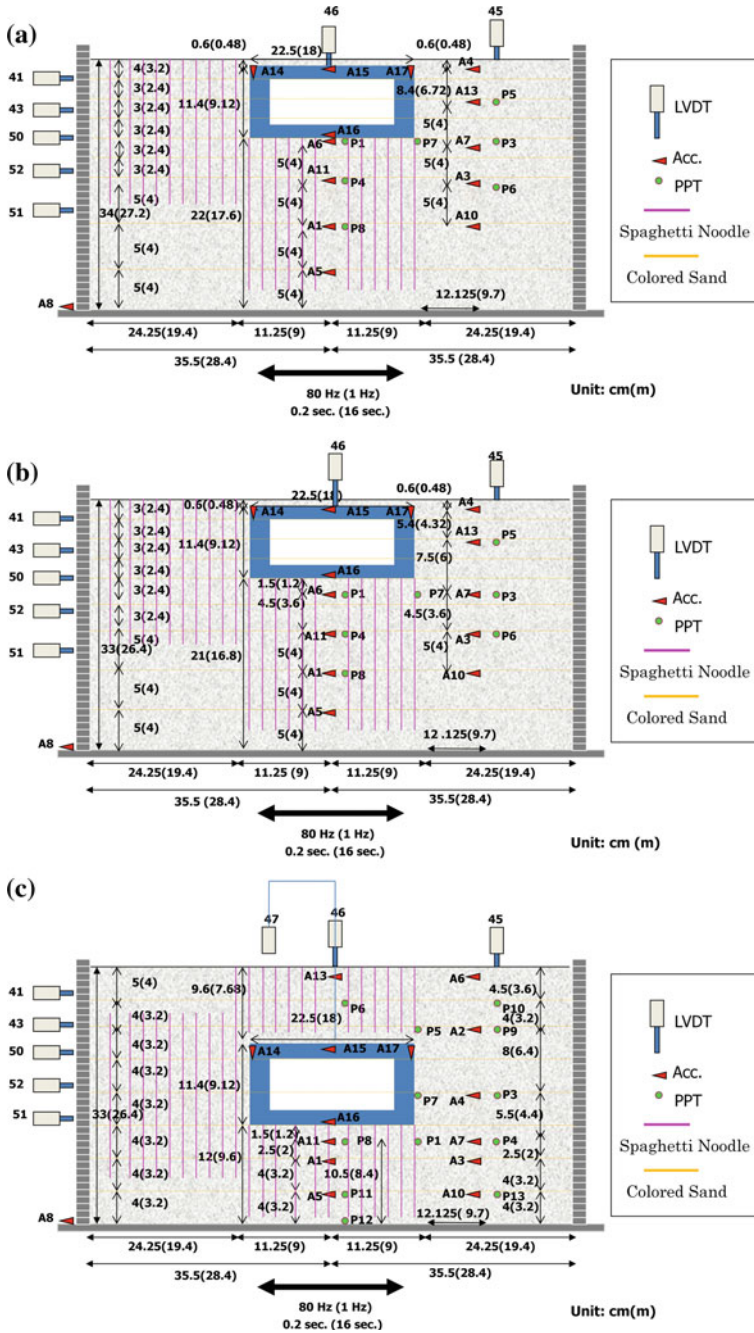
Fig. 2 Testing set-up: **a** Tunnel-1; **b** Tunnel-2; **c** Tunnel-3

Table 2 Test number and testing conditions (all dimensions in prototype)

Test no.	Pore fluid	Embedment depth (m)	Depth of sand deposit (m)	γ_{sat} (kN/m^3)	γ_{tunnel} (kN/m^3)	Max. shaking magnitude (g)	Shaking frequency (Hz)	Shaking elapsed time (s)
Tunnel-1	MCE[a]	0.48	27.2	19.17	9.02	S1:0.13	1	16
						S2:0.23		
Tunnel-2	Water	0.48	26.4	19.04	9.02	S1:0.13	1	16
						S2:0.23		
Tunnel-3	Water	7.68	26.4	19.04	9.02	S1:0.25	1	16

[a]MCE Methocel cellulose ether solution (viscous fluid, kinematic viscosity $\cong$ 40 cSt)

settlements and lateral movements of the rectangular container rings; (3) The seismic responses of the tunnel at the centre of the container and aside the tunnel during shaking; (4) To capture excess pore water dissipation in the far field during the shaking and at the post shaking stage; (5) Several PTTs were also installed beneath the tunnel or at the right-hand side wall of the tunnel to record the pore pressure generation and dissipation around the tunnel; (6) A horizontal PPT array was installed at the bottom of tunnel to capture the pore pressure changes underlying the tunnel, which is the most important thing observed in this study; (7) EPCs were installed on the surfaces of the model tunnel used to measure the earth pressures acting around the tunnel; (8) Several rows of spaghetti were inserted into the sand deposit to investigate the movements of soil near to the model tunnel after tunnel floating.

3   Test Results and Interpretations

Based on the equilibrium of vertical forces acting on a embedded tunnel the safety factor (FS) can be used to evaluate the uplifting of tunnel caused by soil liquefaction (Koseki et al. 1997). The vertical equilibrium in the triggering condition of uplift as shown in Fig. 3 is expressed as:

$$W_s + W_B + Q_s + Q_B = U_s + U_D \tag{1}$$

where $W_s = \gamma_{sat}bh$ = the total overburden weight of soil above the tunnel; $W_B = \gamma_{tunnel}bh$ = the weight of tunnel; $Q_s = H\sigma_{v1}K_o \tan \varnothing$ = the friction resistance of soil above the tunnel; $Q_B = h(\sigma'_{v1} + \sigma'_{v2})K_o \tan \delta$ = the friction resistance of soil along the two side walls of tunnel; $U_s = \gamma_w(h + H)b$ = static pore water pressure at the elevation of tunnel bottom; $U_D = \Delta ub$ = excess pore water pressure at the elevation of tunnel bottom; σ'_{v1} and σ'_{v2} are the effective vertical stresses at the tunnel top and bottom. The safety factor against tunnel uplift can be derived as follows

Fig. 3 Vertical forces on an embedded tunnel during uplifting caused by soil liquefaction
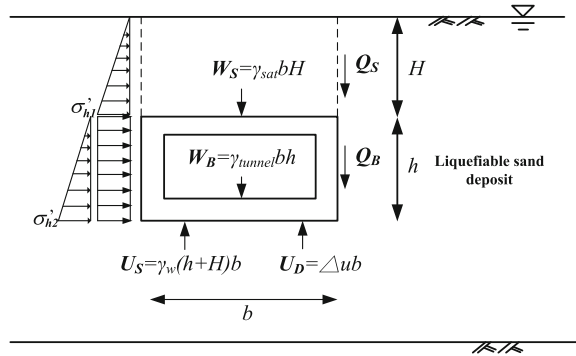
$$FS = \frac{W_s + W_B + Q_s + Q_B}{U_s + U_D} \tag{2}$$

Koseki et al. (1997) examined the relationship between the FS and uplift displacement of box-type structures and concluded that the uplift continues when the FS is less than or almost equal to 1. Equation 2 can be used to evaluate the triggering condition of uplift.

The liquefaction and post-liquefaction behaviours of sand deposits are basically governed by the generation and dissipation of excess pore water pressure. The excess pore water pressure ratio is defined as the measured excess pore water pressure, Δu, divided by the corresponding effective overburden pressure, σ'_v:

$$r_u = \frac{\Delta u}{\sigma'_v} \tag{3}$$

Tunnel-1 and Tunnel-2 are shallowly embedded (0.48 m) in the sand deposit which is saturated with MCE solution (Tunnel-1) and water (Tunnel-2), respectively. Use of viscous pore fluid to replace the water in the sand bed can retard the excess pore water pressure dissipation to simulate the shallow tunnel embedded in the sand deposit having lower permeability (Tunnel-1). Figures 4 and 5 display the time histories of uplift displacement, excess pore water pressure measured at P5 (far away from the tunnel) and acceleration measured at A8 for Tunnel-1 and Tunnel-2 in the S1 event, respectively. The uplift displacement continuously developed even after shaking in Tunnel-1 because of the excess pore water pressure keeping higher. Figure 6a, b displays the time histories of uplift displacement for Tunnel-1 and Tunnel-2 in the S1 and S2 events. The shallow tunnel embedded in the lower permeability deposit would experience the larger uplift displacement. Figure 7 displays the time histories of uplift displacement versus excess pore water pressure for Tunnel-3 ($a_{max} = 0.25g$) and the instrumentation positions and the transducer numbers. Figure 8 displays the time histories of uplift displacement measured at Tunnel-1, Tunnel-2, and Tunnel-3 for comparison. The deeper tunnel (embedded
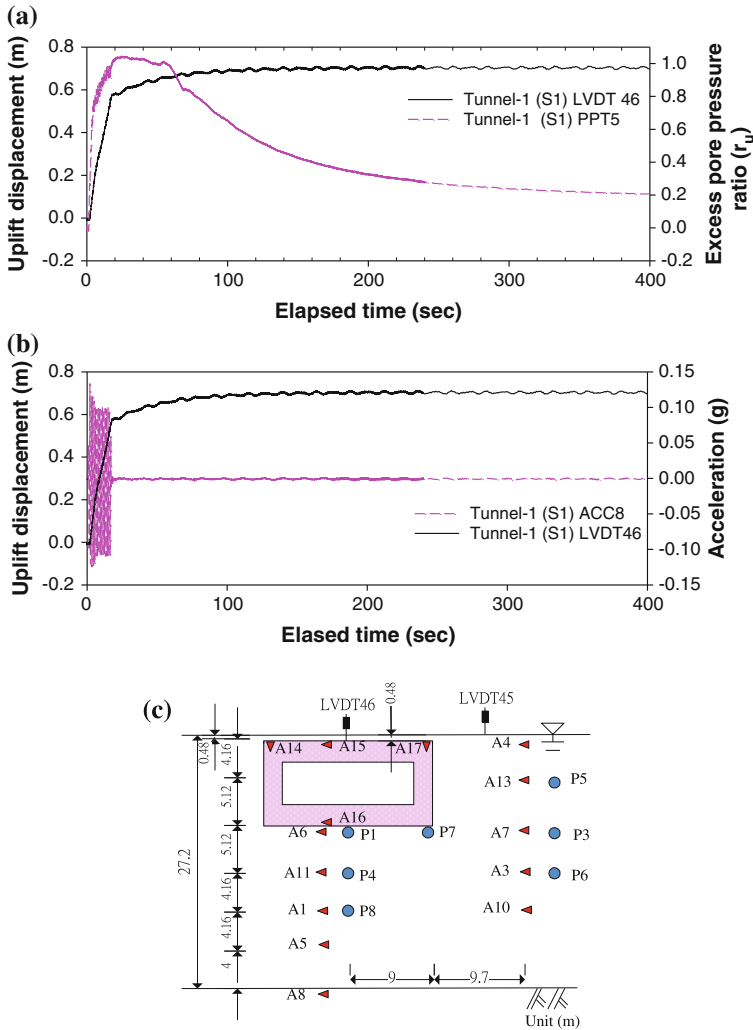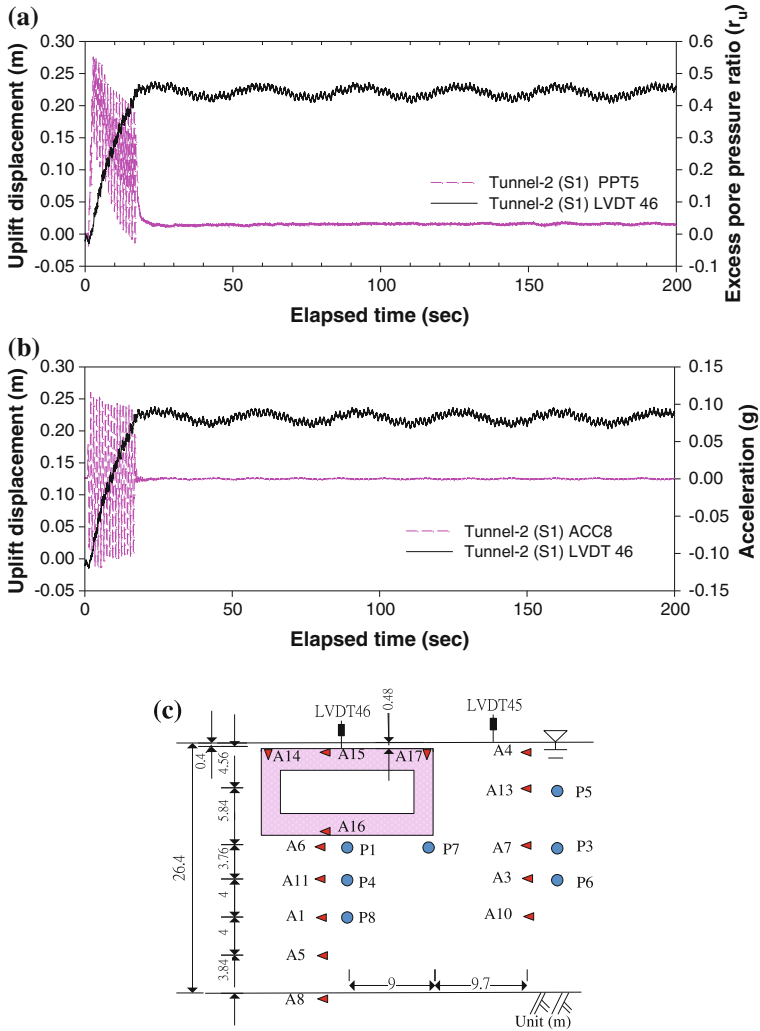
Fig. 4 Time histories of uplift displacement versus excess pore water pressure and acceleration for Tunnel-1 (S1): **a** uplift displacement versus ratio of excess pore water pressure; **b** uplift displacement versus Acceleration; **c** instrumentation positions and transducer number

depth = 7.68 m) experienced the less uplift displacement. Figures 9 and 10 display the developed excess pore water pressures measured at the same elevations but at different positions for Tunnel-1 and Tunnel-3. The installed positions of pore water pressure transducers are shown in Figs. 4c and 7. Figure 11 displays the failure mechanism of tunnel after floating. In Tunnel-1 (shallow tunnel) the measured excess pore water pressure at the position far away from the centre of embedded tunnel is much higher than those measured at the position near to or at the centre of

Fig. 5 Time histories of uplift displacement versus excess pore water pressure and acceleration for Tunnel-2 (S1): **a** uplift displacement versus ratio of excess pore water pressure; **b** uplift displacement versus Acceleration; **c** instrumentation positions and transducer number

tunnel. Larger hydraulic gradients cause the water from the free field flowing to the tunnel bottom. The surrounding soil would squeeze into the tunnel bottom. By contrast in Tunnel-3 the less difference of the magnitude of excess pore water pressures measured at the same elevation below the tunnel bottom are observed. Therefore, the less surrounding sand squeezed into the tunnel bottom and the less uplifting of tunnel is expected. Use of Eq. 2 and measured the excess pore water pressures can calculate the factor of safety as shown in Fig. 12 during and after
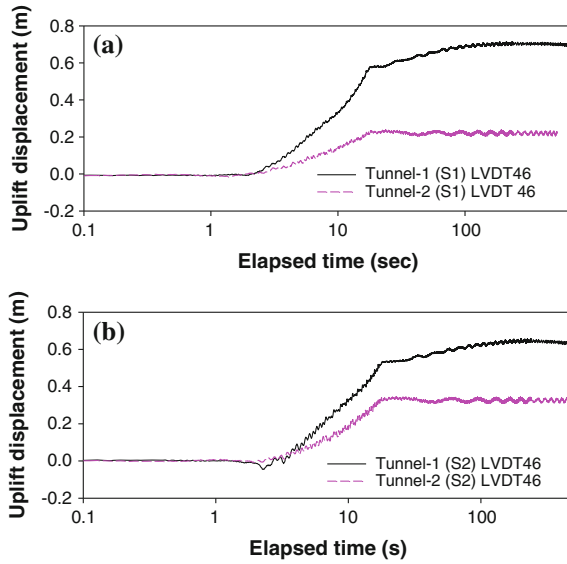
Fig. 6 Time histories of uplift displacement for Tunnel-1 and Tunnel-2 in the event 1 and event 2: **a** event 1 ($a_{max} = 0.13g$); **b** event 2 ($a_{max} = 0.23g$)
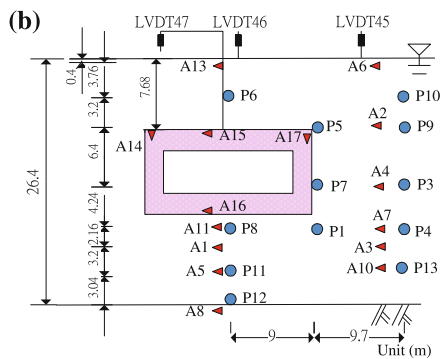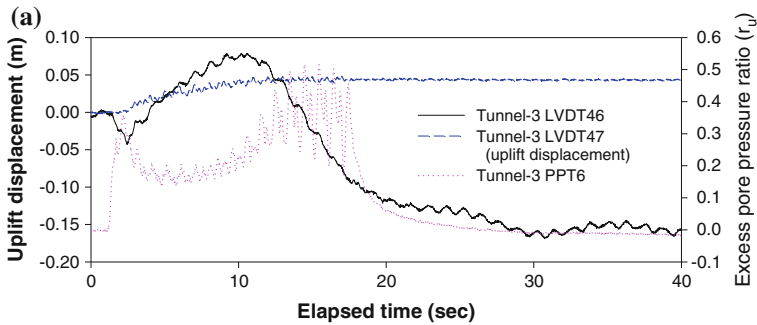

Fig. 7 Time histories of uplift displacement versus excess pore water pressure for Tunnel-3 ($a_{max} = 0.25g$)

Fig. 8 Time histories of uplift displacement for Tunnel-1 (S2, $a_{max} = 0.23g$), Tunnel-2 (S2, $a_{max} = 0.23g$) and Tunnel-3 (S3, $a_{max} = 0.25g$)
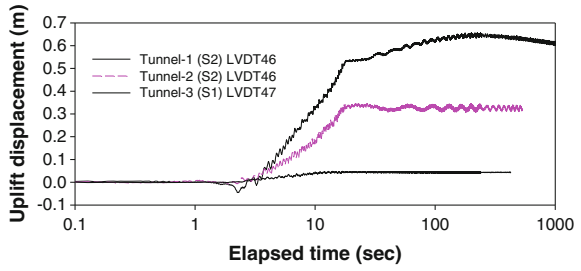
Fig. 9 Time histories of excess pore water pressure at different positions for Tunnel-1 (S2) ($a_{max} = 0.23g$)
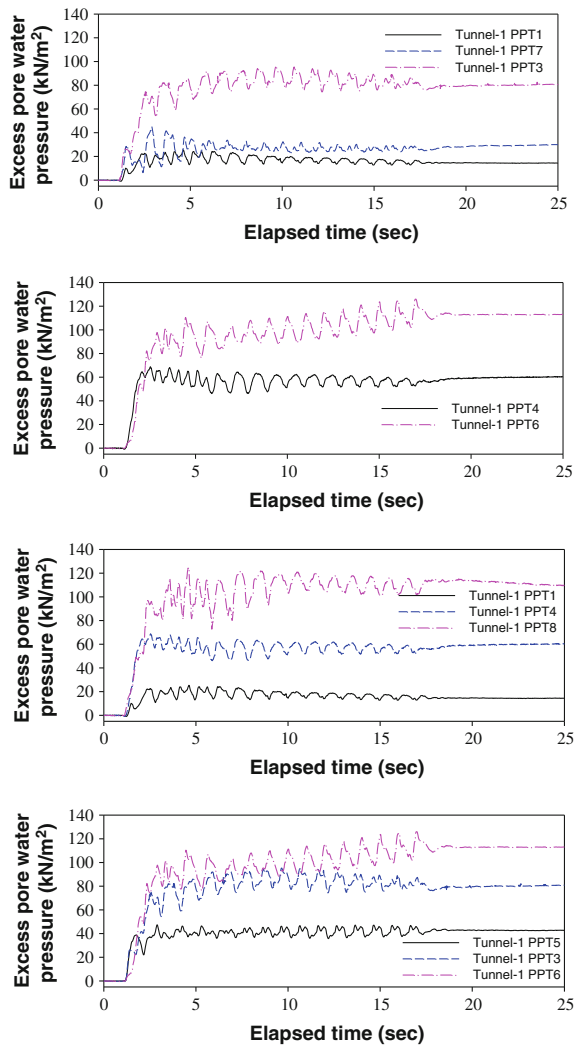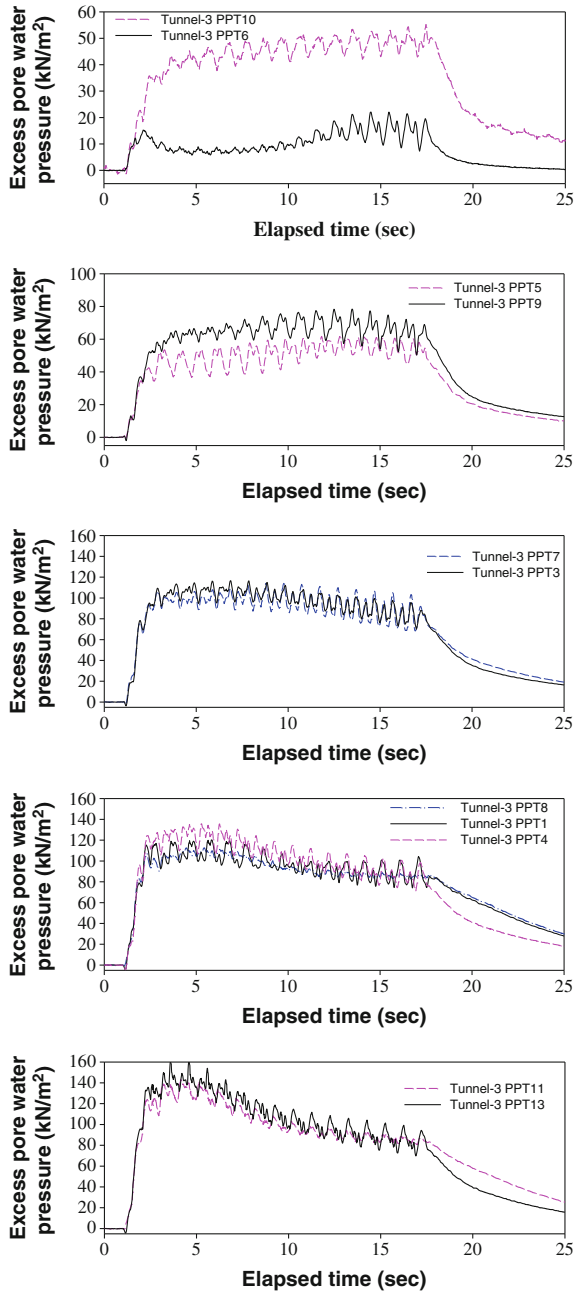
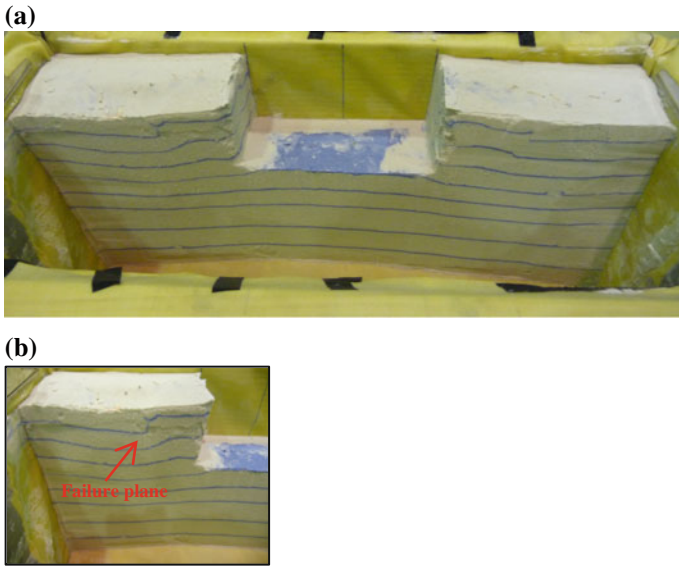**Fig. 10** Time histories of excess pore water pressure at different positions for Tunnel-3 ($a_{max} = 0.25g$)

Fig. 11 The failure mechanism of uplifting for Tunnel-1 after testing: **a** fullview; **b** near view
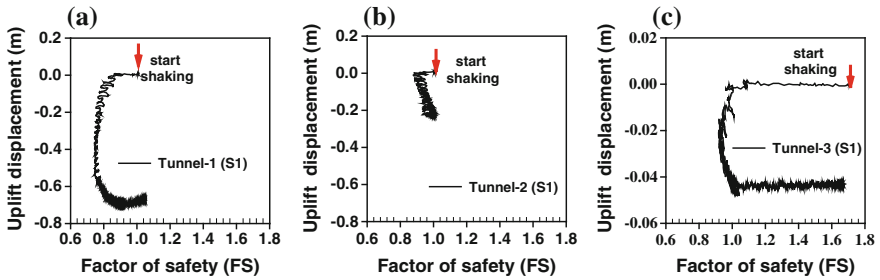

Fig. 12 Magnitude of tunnel uplifting displacement versus Factor of safety during and after shaking: **a** Tunnel-1 (S1); **b** Tunnel-2 (S2); **c** Tunnel-3 (S1)

shaking for Tunnel-1, Tunnel-2, and Tunnel-3. Once the safety factor against uplift (FS) calculated with the proposed method is less than 1 the tunnel would start floating, and after the FS returning to 1 the tunnel stops floating.

4 Summary and Conclusions

According to the model test results, the following conclusions are addressed: (1) The magnitude of tunnel uplift is significantly influenced by the viscosity of pore fluid used and the embedded depth of tunnel. Use of viscous pore fluid would reduce the

rate of excess pore water pressure generation and dissipation and prolong the elapsed time of liquefaction. Therefore, the tunnel embedded in the deeper depth and in the less viscous pore fluid would experience the less magnitude of tunnel uplift during and after shaking. (2) The higher hydraulic gradient between the soil beneath the tunnel bottom and the surrounding soil in the free field became very obvious. The surrounding soil squeezing into the tunnel bottom induced by the higher hydraulic gradient is one of the major causes of tunnel uplifting. (3) The larger magnitude and the longer duration of the base shaking subjected to the liquefiable sand deposit, the larger magnitude of tunnel uplift occurred. (4) Once the safety factor against uplift (FS) calculated with the proposed method is less than 1 the tunnel would start floating during shaking, and after the FS returning to 1 the tunnel stops floating.

References

Abdoun T, Dobry R, Zimmie TF, Zeghal M (2005) Centrifuge research of countermeasures to protect pile foundations against liquefaction-induced lateral spreading. J Earthquake Eng 9 (1):105–125

Chian SC, Madabhushi SPG (2010) Influence of fluid viscosity on the response of buried structures in earthquakes. In: 7th international conference of physical modelling in geotechnics, pp 111–115

Chian SC, Madabhushi SPG (2012) Effect of buried depth and diameter on uplift of underground structures in liquefied soils. Soil Dyn Earthq Eng 41:181–190

Koseki J, Matsuo O, Koga Y (1997) Uplift behavior of underground structures caused by liquefaction of surrounding soil during earthquake. Soils Found 37(1):97–108

Lee CJ (2005) Centrifuge modeling of the behavior of Caisson-type quay walls during earthquake. Soil Dyn Earthq Eng 25(2):117–131

Lee CJ, Wei YC, Kou YC (2012) Boundary effects of a laminar container in centrifuge shaking table tests. Soil Dyn Earthq Eng 34(1):37–51

Tobita T, Kan GC, Iai S (2010) Uplift behavior of buried structures under strong shaking. In: 7th international conference of physical modeling in geotechnics, pp 1439–1444

Tobita T, Kan G-C, Iai S (2012) Estimation of liquefaction-induced manhole uplift displacements and trench-backfill settlements. J Geotech Geoenvironmental Eng ASCE 138(4):491–499